JACS
JOURNAL OF THE AMERICAN CHEMICAL SOCIETY

Article

pubs.acs.org/JACS

Energy Transfer Between Squaraine Polymer Sections: From *Helix* to *Zigzag* and All the Way Back

Christoph Lambert,*[,†,‡] Federico Koch,[§] Sebastian F. Völker,[†] Alexander Schmiedel,[†] Marco Holzapfel,[†] Alexander Humeniuk,[§] Merle I. S. Röhr,[§] Roland Mitric,[§] and Tobias Brixner*[,‡,§]

[†]Institut für Organische Chemie, [‡]Center for Nanosystems Chemistry (CNC), and [§]Institut für Physikalische und Theoretische Chemie, Universität Würzburg, Am Hubland, 97074 Würzburg, Germany

Supporting Information

ABSTRACT: We provide a joint experimental and theoretical study of squaraine polymers in solution. The absorption spectra show evidence that two different conformations are present in the polymer: a *helix* and a *zigzag* structure. This unique situation allows investigating ultrafast energy-transfer processes between different structural segments within a single polymer chain in solution. The understanding of the underlying dynamics is of fundamental importance for the development of novel materials for light-harvesting and optoelectronic applications. Here, we combine femtosecond transient absorption spectroscopy with time-resolved 2D electronic spectroscopy in order to demonstrate that ultrafast energy transfer within the squaraine polymer chains proceeds from initially excited *helix* segments to *zigzag* segments or vice versa, depending on the solvent as well as on the excitation wavenumber. These observations contrast other conjugated polymers such as MEH-PPV where much slower intrachain energy transfer was reported. The reason for the very fast energy transfer in squaraine polymers is most likely a close matching of the density of states between donor and acceptor polymer segments because of the very small reorganization energy in these cyanine-like chromophores.

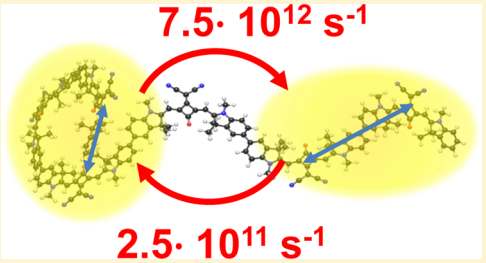

INTRODUCTION

Energy transfer in conjugated polymer chains is an issue of fundamental importance for the development of organic solar cells and various optoelectronic devices.[1−10] While most low-molecular-weight systems exhibit structural flexibility that is fast even on time scales of nanoseconds, polymers may behave totally differently due to their higher molecular weight, which leads to slower structural dynamics. Thus, in polymer solutions a distribution of conformers might be present, which may influence the fast dynamical electronic processes that occur in optoelectronic devices such as exciton diffusion or charge migration.[11−21] For this reason it is extremely difficult to gain insight into the relation of electronic processes in conjugated polymers and their microscopic or superstructure in solution and in the solid state.[22] Recently Scholes et al. addressed this issue very elegantly by investigating MEH-PPV in its stretched form in $CHCl_3$ solution in comparison to its coiled nanoparticle form in aqueous solution.[23] These authors could show that after excitation the coherence persists for some 100 fs in the stretched polymers. In contrast, in the coiled nanoparticles, interchain energy migration dominates. The latter is probably the more relevant scenario for condensed phases of MEH-PPV and related conjugated polymers. There it was found that interchain energy transfer is faster than intrachain energy transfer.[24] This is most likely caused by the shorter interchain distance in condensed phase and by the face-to-face orientation of localized transition moments. Some of us also determined the interplay between local morphology and energy transfer in MEH-PPV for varying temperatures around the phase-transition point using ultrafast spectroscopy.[25,26]

Thus, the study of dynamic processes in polymer strands of defined structure in solution is of great importance for a better understanding of the bulk material.[27−31] However, what is lacking is information about the influence of different local structures on photoinduced processes within a single polymer strand. These data are decisive because conjugated polymers in the solid state will usually adopt a variety of local structures that are hard to control in a deliberate way. The resulting interchain processes are expected to overlap dynamically and spectroscopically with intrachain processes, making them difficult to discriminate. One way of solving this dilemma is gaining information under dilute conditions in solution phase which will exclude all interchain processes. We have recently undertaken a series of studies concerning the static and dynamic optical properties of polymeric squaraine dyes in solution.[32−36] In this context we found a polymer whose relative amount of local superstructure (*helix* and *zigzag*) within a single polymer strand depends on the solvent. Thus, this polysquaraine opens a unique chance to study the above-mentioned intrachain processes.

Both polymeric and low-molecular-weight squaraine dyes gained much attention in recent years[37] because of their typical cyanine-like behavior, i.e., strong and usually narrow absorption

Received: April 14, 2015
Published: May 28, 2015

DOI: 10.1021/jacs.5b03644
J. Am. Chem. Soc. 2015, 137, 7851−7861

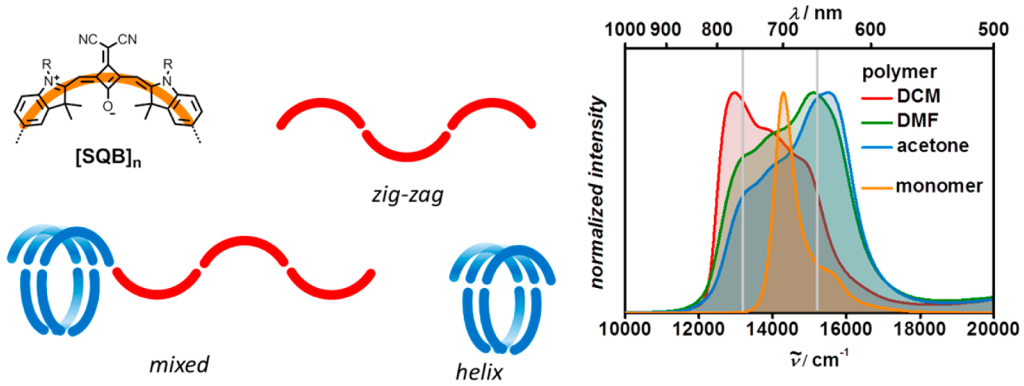

Figure 1. Proposed polymer structures of $[SQB]_n$ and absorption spectra in diverse solvents. The gray bars in the absorption spectra indicate the laser excitation wavenumbers.

in the red part of the visible light spectrum along with strong fluorescence.[38−43] These properties allow many applications from dye-sensitized solar cells and organic photovoltaic applications[32,44−66] to ion sensors[67−71] and biolabeling.[72−80] Unlike conjugated polymers that are based on very small monomers such as styrene (e.g., MEH-PPV) or thiophene (e.g., P3HT) and whose polymer properties are totally different from those of the monomers,[81] squaraine homo- and copolymers are based on squaraine dyes which already show a strong absorption in the red region of the visible spectrum.[32−36,82] The optical properties of the squaraine polymer, although distinct from those of the monomeric dye, can be explained by exciton coupling of localized squaraine chromophore transition moments which in general leads to broadened and red-shifted spectra reflecting the excitonic manifold of states. Accordingly, the red-shifts into the NIR spectral region and changes of absorption band shapes were discussed previously.

For the squaraine homopolymer $[SQB]_n$ (see Figure 1) we found evidence that the superstructure in solution depends on the solvent.[36] Thus, in some solvents (e.g., DCM, $CHCl_3$) stretched polymer chains dominate which leads to a pronounced red-shifted absorption (J-aggregate behavior = head-to-tail arrangement of transition moments) compared to the monomer absorption, while in others (e.g., acetone), the polymers mostly adopt a *helix* conformation which displays a blue-shifted most intense absorption (H-aggregate behavior = face-to-face arrangement of transition moments) of the exciton manifold.[33] In DMF, obviously mixtures of both superstructures are present within one polymer strand. The assignment to specific structural motifs was derived from a variety of calculated (semiempirical AM1 method) structural models whose computed absorption spectra (INDO method) agree with the measured spectra when, e.g., the spectra of *helix* and of *zigzag* structures with different ratios are superimposed. While this picture is certainly highly simplistic, it is able to explain the basic spectral features very well. Further support on this structural assignment with the help of computed absorption spectra will be given below based on more elaborate DFT calculations.

In this work, we will assess the photoinduced dynamics of the $[SQB]_n$ polymer in two different solutions, in DCM, where predominantly stretched polymer chains prevail, and in DMF, where, besides stretched sections, the polymer possesses mainly helix sections. By transient absorption pump−probe spectroscopy,[83] we will show that the dynamics are significantly different in these two solvents which can be traced back to the different superstructure. Finally, support for the interpretation is given by coherent two-dimensional (2D) electronic spectroscopy, as it separates signal contributions into excitation and detection energies.[84−87] With 2D spectroscopy we monitor the energy relaxation of excited chromophores within different structural domains.

EXPERIMENTAL SECTION

Spectroscopic Methods. For all spectroscopic experiments squaraine homopolymer $[SQB]_n$ with M_w = 46700, PDI = 1.8, and X_n = 36 was dissolved in DMF or DCM to achieve an optical density OD ≈ 0.3 at the respective excitation wavenumber.

Transient absorption spectra of the squaraine polymer were obtained by pumping $[SQB]_n$ with ca. 140 fs laser pulses (1 kHz) generated by an amplified Ti:sapphire oscillator (fundamental 800 nm, 12500 cm^{-1}) and an OPA for generating the appropriate excitation wavenumber (13200 and 15200 cm^{-1}) and by probing with a white-light continuum generated with a small portion of the fundamental focused in a CaF_2 crystal. The instrument response was ca. 110 fs as determined by fitting the coherent artifact signals of the pure solvent. In order to prove the absence of multiphoton absorption effects in the transient spectra, we performed experiments at different laser pulse energies which showed linearity up to 200 nJ $pulse^{-1}$ (see Supporting Information (SI)). Thus, all subsequent measurements were done at either 50 or 100 nJ $pulse^{-1}$.

Transient absorption data were analyzed with the global and target analysis program GLOTARAN based on the statistical fitting package TIMP.[88−90] This procedure accounts for the chirp (by third-order polynomial correction) and the coherent artifact (by fitting the instrument response). However, some weak residual signals (Raman signals) of the coherent artifact are still visible in the fastest deconvoluted spectral component. The results of a parallel fitting model are presented in the wavelength domain as decay-associated difference spectra (DADS).[91] Each DADS corresponds to the wavelength-dependent amplitudes of one exponential decay component. Furthermore, results of a target model are presented with species-associated difference spectra, (SADS) each of which belongs to one species that may be populated or depopulated by several paths.

Coherent optical 2D experiments were performed in an inherently phase-stable 2D setup, described extensively elsewhere.[92] Briefly, excitation pulses centered at 13700 cm^{-1} (730 nm) were realized by using a commercial noncollinear optical parametric amplifier (NOPA, TOPAS-white, Light Conversion Ltd.) pumped by a commercial Ti:sapphire regenerative-amplifier laser system (Spitfire Pro, Spectra Physics, 800 nm, 120 fs, 1 kHz). Pulse durations at the sample position were 22 fs for the experiments in DCM and DMF, as determined from SHG-FROG in a 10 μm β-barium borate (BBO) crystal. For each population time T (time delay between pulses 2 and 3), the coherence time τ (time delay between pulses 1 and 2) was varied between τ = ±120.69 fs in steps of $\Delta\tau$ = 4.47 fs. Real-valued 2D spectra, reflecting

DOI: 10.1021/jacs.5b03644
J. Am. Chem. Soc. 2015, 137, 7851−7861

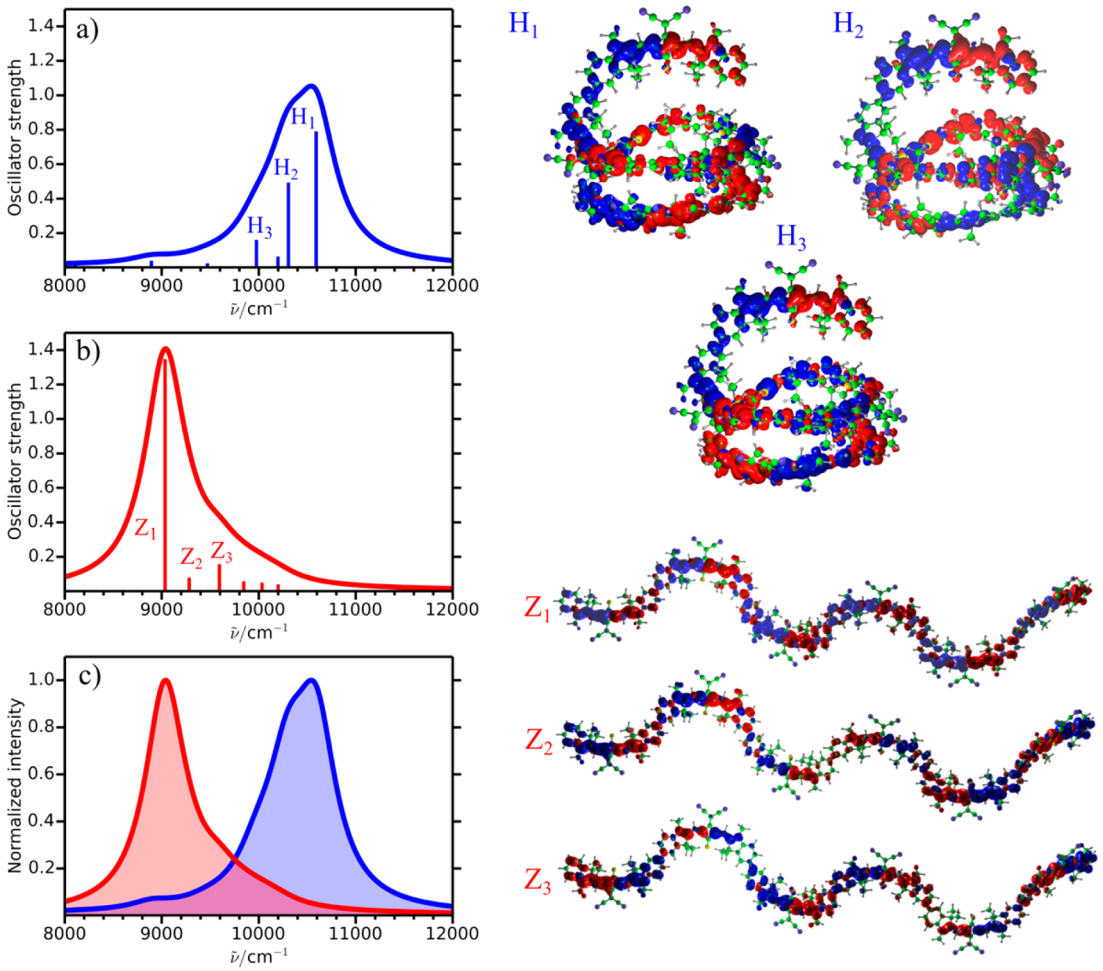

Figure 2. Calculated absorption spectra of the (a) *helix* and (b) *zigzag* superstructure of a model SQB hexamer. The labels H_{1-3} and Z_{1-3} denote the three most intense transitions for the *helix* and *zigzag* conformer, respectively. (c) Comparison of the theoretical normalized absorption spectra for both conformers. The transition densities for the three most intense transitions of both conformers are presented on the right-hand side of the figure.

the change in absorption, were obtained by phasing with transient absorption data within the same experimental setup using beam 3 as a probe. Optical signals were spectrally dispersed and detected via a spectrograph (Acton SP2500i) equipped with a CCD camera (Princeton Instruments Pixis 2k).

Computational Methods. The optical spectra of the *zigzag* and *helix* form of the model SQB hexamer were calculated using the recently introduced long-range-corrected tight-binding time-dependent density functional theory (lc-TDDFTB).[93] Since the details of the lc-TDDFTB method have been published elsewhere,[93] we only provide a brief summary here. The lc-TDDFTB method has been introduced as an approximate and highly efficient alternative to the long-range-corrected TDDFT,[94] which is applicable to much larger systems containing up to several thousands of atoms. This method introduces the long-range correction to the linear response version of the time-dependent density functional tight binding method (TDDFTB)[95] by adding an exact Hartree−Fock exchange term, which is switched on at large distances, to the ground-state DFTB Hamiltonian[96] as well as to the TDDFTB coupling matrix. We wish to emphasize that the inclusion of the long-range correction is mandatory in order to exclude the contamination of the spectra by spuriously low charge-transfer states, which typically occur in conventional TDDFT and TDDFTB and might pose a serious problem, in particular in multichromophoric oligomers and polymers.

Based on the geometries obtained from the semiempirical AM1 calculations,[36] the ground-state electronic structure has been first calculated using the self-charge-consistent DFTB with the long-range correction included into the ground-state Kohn−Sham (KS) Hamiltonian. This provides occupied and virtual KS orbitals, which are subsequently used to calculate the optical spectra. The latter are obtained by solving Casida's equation with a long-range-corrected coupling matrix. The solution of the linear response problem provides the excitation energies and excitation coefficients which were used to calculate the transition dipole moments and oscillator strengths of the optical transitions. For this purpose we employ Slater−Koster tables for the dipole matrix elements between valence orbitals, which provides a more accurate description of the oscillator strengths than the commonly used Mulliken transition charge approximation. The character of the excited states has been analyzed by computing the electronic transition densities. The expected accuracy of the lc-TDDFTB approach is comparable to the full long-range-corrected TDDFT (CAM-B3LYP). Our tests on a large suite of molecules gave rise to an average error of the transition energies for excited states with local or delocalized character between 0.3 and 0.4 eV. While not fully quantitative, this allows us to reproduce the overall shape of the experimental spectra reasonably well and to provide the assignment of the spectral features to the structural motifs.

RESULTS AND DISCUSSION

Computations. The strongest absorption band of the *helix* conformer is located at 10600 cm^{-1} and is accompanied by two weaker bands at 10300 and 9980 cm^{-1} (Figure 2a). These three bands belong to the first exciton manifold, which arises due to the electronic coupling between the first excited state of six individual monomeric units. The excitonic character is

DOI: 10.1021/jacs.5b03644
J. Am. Chem. Soc. 2015, 137, 7851−7861

illustrated by the calculated transition densities shown in Figure 2 (H_1–H_3). The transition densities for all three states are strongly delocalized along the *helix* structures and differ by the signature (phase) on the individual monomeric units. Since in the *helix* structure, the individual chromophores are stacked, a H-type (face-to-face) coupling occurs leading to the highest intensity of the most blue-shifted intense band H_1. We also note that the first excitonic manifold consists of six transitions with a bandwidth (= highest-to-lowest energy transition) of ca. 1750 cm^{-1} (cf. Figure 2a).

In contrast, the absorption spectrum of the extended *zigzag* conformer exhibits a most intense transition which is strongly red-shifted with respect to the most intense transition of the *helix* structure and is located at 9000 cm^{-1}. The intense band is accompanied by two weaker peaks at 9280 and 9600 cm^{-1} (Figure 2b). The transition densities for the three lowest-lying intense bands are presented in Figure 2 (Z_1–Z_3). Again, the transition densities are fully delocalized over the extended structure and reflect the coupling of transition dipole moments on individual monomers. For example, in the most intense transition Z_1 all monomers are coupled in a head-to-tail manner with transition dipoles pointing in the same direction, which is a characteristic J-aggregate behavior. The total bandwidth of the first excitonic band is ca. 1200 cm^{-1}, lower than for the *helix* structure. The smaller bandwidth of the *zigzag* structure is in agreement with the experimental findings.

In order to emphasize the spectral differences between the *helix* and the *zigzag* superstructure, we also present the theoretical normalized spectra of both species in Figure 2c. It can be clearly seen that the spectrum of the extended structure is strongly red-shifted with respect to the one for the *helix* structure. The theoretical spectra can be compared with the experimental spectra of the SQB polymers presented in Figure 1 leading to the assignment of the spectrum in DCM to the predominant *zigzag* structure. In acetone or DMF, the theoretical calculations support the assignment to the predominant *helix* structure. This assignment is further supported by calculations on the *zigzag* and helical conformations of larger oligomers containing N = 12 and 22 units, which are presented in Figure 3a,b, respectively. The spectra of larger oligomers are slightly blue-shifted, and the difference of the maxima of the excitonic bands of *zigzag* and *helix* structures becomes significantly larger. For N = 12 this difference is 3000 cm^{-1} and increases to around 4000 cm^{-1} for the N = 22 oligomer, which is in a good agreement with the experimental spectra in Figure 1

Transient Absorption. In DCM where the $[SQB]_n$ polymer adopts mainly the elongated *zigzag* structure, we performed two different pump–probe experiments: In the first experiment (hereafter called experiment 1), we pumped the sample at 13200 cm^{-1}, where the *zigzag* structure shows the highest extinction coefficient and, thus, will be predominantly excited. Accordingly, right after the excitation, the transient spectra (Figure 4a) show a strong ground-state bleaching (GSB) at ca. 13000 cm^{-1}, which experiences a little red-shift within the first ps. Much weaker GSBs are seen at ca. 15000 and ca. 25000–26000 cm^{-1}. There is also a broad but weak excited-state absorption (ESA) between 16000 and 24000 cm^{-1}. All of these signals decay with only little changes of their relative intensities. In Figure 4, the time traces directly reflect the approximate population of excited *zigzag* segments (time trace at 12900 cm^{-1}) and excited *helix* structure (time trace at 15200 cm^{-1}). This assumption is supported by the TDDFT

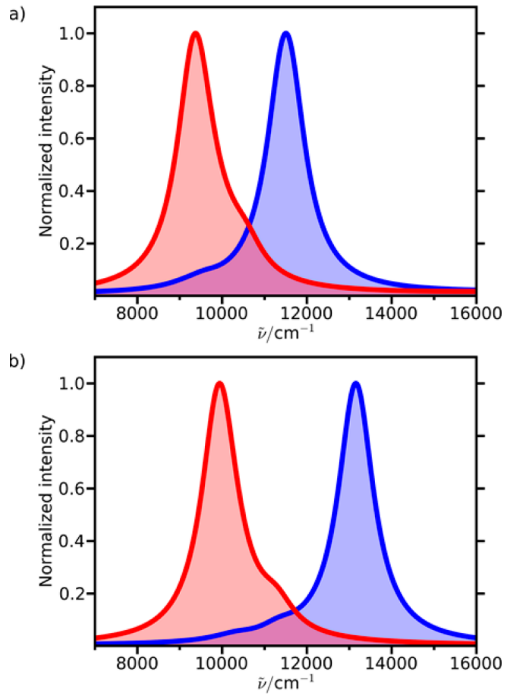

Figure 3. Calculated absorption spectra of the squaraine (a) 12mer and (b) 22mer. Red and blue curves correspond to the *zigzag* and *helix* conformations, respectively. The peak intensities have been normalized to unity, and the lines have been broadened by a Lorentzian function with the width of 1000 cm^{-1}.

computations (see Figure 3), which show little absorption (= GSB in the transient absorption spectra) of the *helix* structure at the maximum absorption of the *zigzag* structure and vice versa. These observations support that almost exclusively *zigzag* chains have been excited which relax to the ground state.

In the second experiment (= experiment 2), we pumped the same sample at 15200 cm^{-1}, which excites those few polymer sections which possess a *helix* structure. While the transient spectra (Figure 4b) are generally similar to those of the first experiment (13200 cm^{-1} excitation), a closer inspection shows some delicate differences: again, the strongest GSB is at 13000 cm^{-1}, but there is now also a pronounced GSB at 15000 cm^{-1}. The former indicates excitation of *zigzag*, the latter of *helix* structures. However, the 15000 cm^{-1} GSB decays more rapidly within the first ps than that at 13000 cm^{-1}. This rapid decay can be seen in the corresponding time traces in Figure 4b (at 15200 cm^{-1}, marked with a red circle). From then on the transient spectra look very similar to those of experiment 1. Thus, in both experiments after ca. 1 ps we end up with excited *zigzag* polymer strands, which indicates that energy transfer from the helix segments to the *zigzag* segments within one polymer strand must have occurred. The alternative explanation, parallel excitation of *helix* and *zigzag* segments and relaxation within their respective exciton manifold, can be ruled out because this could not explain the rapid and strong amplitude decay of the 15200 cm^{-1} signal. At this point, we stress that the sample solutions are very diluted which excludes energy transfer between different polymer strands.

In order to elucidate the impact of structure on the photoinduced dynamics, we also performed two pump–probe experiments of the $[SQB]_n$ polymer in DMF solution. Here, the polymer strands possess predominantly a *helix* conformation. Excitation at 13200 cm^{-1} (= experiment 3) yields transient

DOI: 10.1021/jacs.5b03644
J. Am. Chem. Soc. 2015, 137, 7851–7861

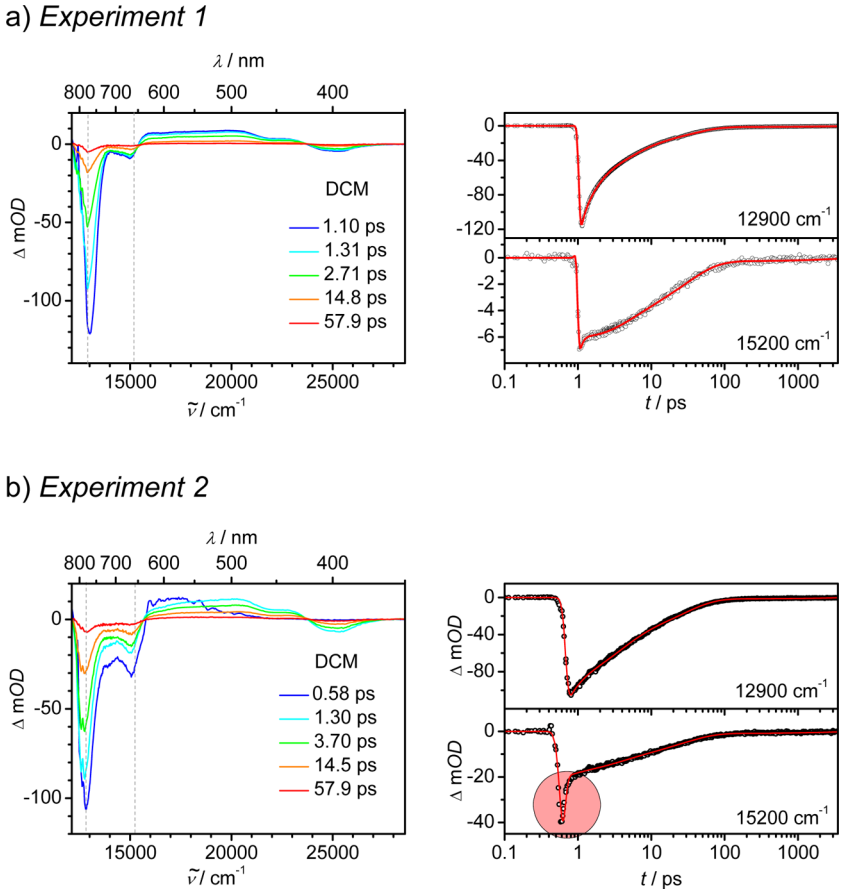

Figure 4. Selected transient absorption spectra (stray light and chirp corrected; early spectra are given in blue, later spectra in red) and selected time traces with global fit (red lines) of $[SQB]_n$ in DCM with excitation at (a) 13200 and (b) at 15200 cm^{-1} pump wavenumbers. The wavenumbers of the time traces are given by gray dashed lines in the spectra diagrams.

spectra (see Figure 5a) with a strong GSB at ca. 13000 cm^{-1} together with ESA and GSB signatures at lower wavenumber similar to the DCM experiments. The strong GSB again shows a little red-shift and decays to ca. 2/3 of the initial intensity within the first ps. At the same time another GSB at ca. 15000 cm^{-1} grows in, as can easily be seen in the time traces at 15600 cm^{-1} (marked with a red circle in Figure 5a). This leads to a reversal of relative GSB intensities at 13000 and 15000 cm^{-1} within the first 10 ps. After 20 ps, the GSB at 13000 cm^{-1} has almost disappeared. The transient spectra at $t > 20$ ps thus indicate almost exclusive population of excited *helix* structures. In contrast to the results in DCM, the observations made in DMF indicate energy transfer from *zigzag* to *helix* segments within one polymer strand. In the second pump−probe experiment in DMF (= experiment 4), the sample was pumped at 15200 cm^{-1}, thus exciting *helix* segments. Initially, the transient spectra show both a very intense GSB at ca. 15600 cm^{-1} and a prominent GSB at ca. 13000 cm^{-1}. The former decays rapidly within the first ca. 100 fs (time trace at 15600 cm^{-1}, Figure 5b) and from then on more slowly. The GSB at ca. 13000 cm^{-1} behaves differently. It does not show the very rapid decay at the beginning, but decays overall much faster at later times than the 15600 cm^{-1} GSB. In the end, the transient spectra are left with a strong GSB at ca. 15600 cm^{-1}, again indicating almost exclusive excited-state population of *helix* structures.

Global Analysis. Taken together, the above sketched experiments indicate energy-transfer processes from *helix* to *zigzag* segments (experiment 2) and from *zigzag* to *helix* structures (experiment 3). This can only be understood if the lowest excited state has *zigzag* structure in DCM but *helix* structure in DMF. In order to assess the number of spectral components to the transient spectra, we performed a global analysis of the transient map (absorbance change as a function of wavenumber and time) using the GLOTARAN software. This analysis gave five components in all cases, as depicted in Figure S3 in the SI in the form of decay-associated difference spectra (DADS, parallel decay mechanism). However, the fifth component has a very small amplitude in all cases and was therefore disregarded in further discussions which can be found in the SI. At this point we stress that the underlying assumption in the global analysis of a finite number of discrete electronic states is a rather crude approximation given the structural complexity of the polydisperse polymer. Thus, in our heuristic model we employed the minimum number of spectral components which gave a satisfactory fit on the expense of unambiguousness of the spectral shape of the DADS and of the SADS in the target model. This means that some spectra may show "mixed" character of both *helix* and *zigzag* structure to a varying degree, although this would not be expected for "pure" SADS.

Target Analysis. The above presented data (Figures 4 and 5 and the DADS in SI) and evaluated information were used to develop a kinetic model for the experiments in DCM and in DMF to which the transient data were globally fitted (target analysis). In these target models we assumed an energy transfer

DOI: 10.1021/jacs.5b03644
J. Am. Chem. Soc. 2015, 137, 7851−7861

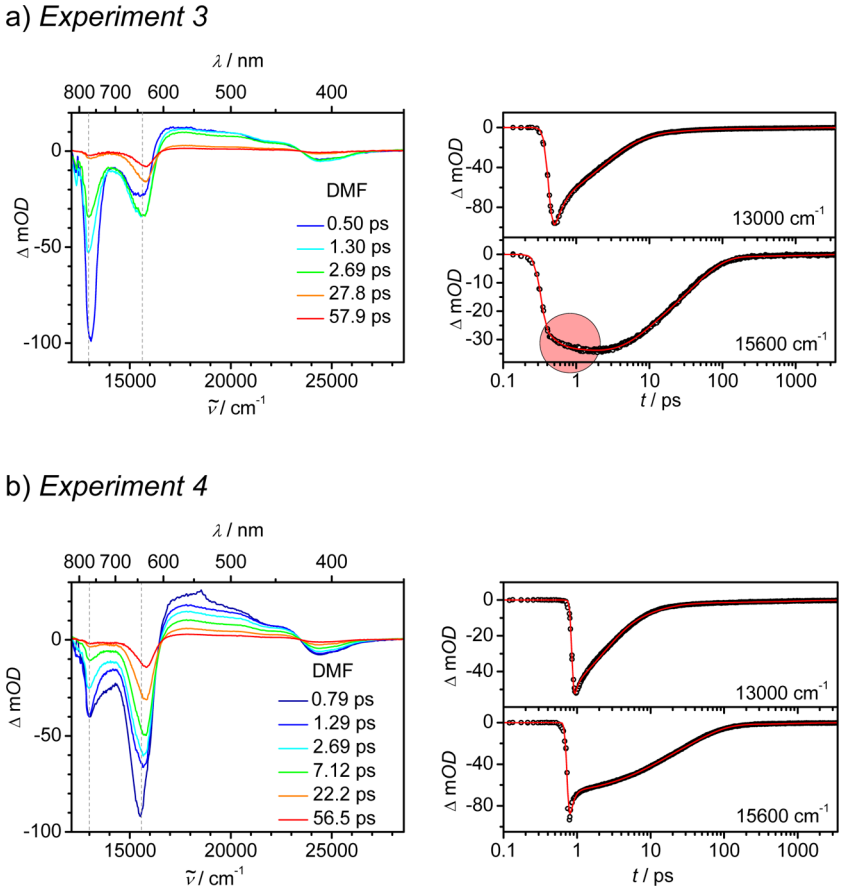

Figure 5. Selected transient absorption spectra (stray light and chirp corrected; early spectra are given in blue, later spectra in red) and selected time traces with global fit (red lines) of $[SQB]_n$ in DMF with excitation at (a) 13200 and (b) at 15200 cm^{-1} pump wavenumbers. The wavenumbers of the time traces are given by gray dashed lines in the spectra diagrams.

from *helix* to *zigzag* segments (see experiment 2) and *zigzag* to *helix* segments (see experiment 3) and both processes for experiment 4. Furthermore, we assumed that the extinction coefficients of all species at ca. 18800 cm^{-1} are equal for all transient species, as ESA to higher lying states should have the same extinction coefficient. This requires to introduce additional pathways connecting the transient species and to adjust the efficiencies (see Tables S1 and S2 in the SI) for each particular pathway. The outcome of these target analyses are SADS, which are given together with the kinetic pathways in Figure 6 for DCM and in Figure 7 for DMF.

For experiment 2, the target analysis in Figure 6 indicates a parallel excitation of *helix* and *zigzag* structure in a 60%:40% ratio. These states are labeled "A" and "Y" in Figure 6. The SADS of A show prominent bleaching signals at 15200 cm^{-1} (black spectrum in the left inset in Figure 6). Species Y relaxes in an ultrafast process to B and is therefore not visible in the spectra. Species A has a lifetime of 70 fs. This could mean either that it relaxes first within the exciton manifold to X from which ultrafast ($\tau \ll 70$ fs) energy transfer to B occurs (in that case X is also not visible in the spectra because of its low intermediate concentration) or that A first undergoes energy transfer with τ = 70 fs to Y and then relaxes in an ultrafast process. We cannot discriminate between both cases (given by dashed and dotted lines in Figure 6) by kinetic methods, but we can give an upper bound for the rate of energy transfer from *helix* to *zigzag* structure with 1/(70 fs) ($k_{A\rightarrow B} = 1.4 \times 10^{13}$ s^{-1}). However, we will give below evidence that the latter mechanism (dashed lines) is at work (see experiment 4). In either case, the relaxation process within the exciton manifold from A into B can be followed by the spectral changes of the ESA around 18200−25000 cm^{-1}. The SADS of B−D are quite similar to each other with a prominent bleaching at ca. 13000 cm^{-1}, which indicates excited *zigzag* population. From B, two structural relaxation processes lead via C and D with τ(B) = 340 fs and τ(C) = 3.4 ps by depopulation with τ(D) = 28 ps into the ground state. The efficiencies for the latter processes can be found in Table S1 in the SI.

Direct excitation of the *zigzag* structures of the squaraine polymer in DCM at 13200 cm^{-1} in experiment 1 is followed by relaxation within the exciton manifold from B′ to B with τ = 110 fs. This process goes along with spectral changes of the ESA between 20000 and 25000 cm^{-1} (see right inset in Figure 6). From then on, structural relaxation and excited-state depopulation processes occur very similarly to the ones in experiment 2 concerning their SADS and the associated lifetimes.

In DMF excitation of the *zigzag* segments at 13200 cm^{-1} (experiment 3) yields first an SADS with a very strong GSB at ca. 13000 cm^{-1} (black spectrum of B′ in the right inset in Figure 7) and subsequent SADS (spectra of B−D in the right inset in Figure 7) with decreasing GSB at this wavenumber but increasing GSB at ca. 16000 cm^{-1} (see right inset in Figure 7). Unlike experiment 1 and 2 in DCM where the SADS of species B−D were spectrally very similar, in DMF the relative intensity of the GSB at 13000 and at 16000 cm^{-1} changes stepwise going

DOI: 10.1021/jacs.5b03644
J. Am. Chem. Soc. 2015, 137, 7851−7861

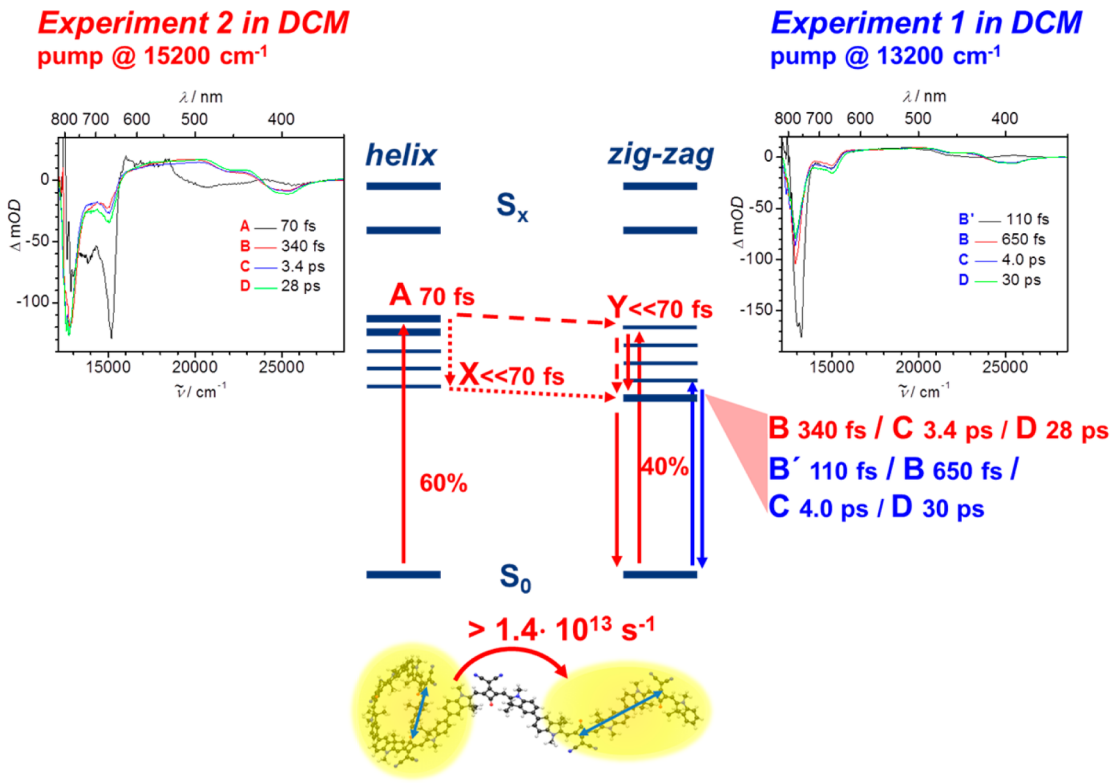

Figure 6. SADS of $[SQB]_n$ in DCM at 15200 cm^{-1} (left) with parallel excitation of *helix* and *zigzag* segments in a 60%:40% ratio and at 13200 cm^{-1} (right) pump energy with 100% excitation of *zigzag* sections. State diagrams (the number of exciton states is arbitrary) of *helix* and *zigzag* sections (middle). Assignments and data given in red pertain to experiment 2, and those given in blue pertain to experiment 1.

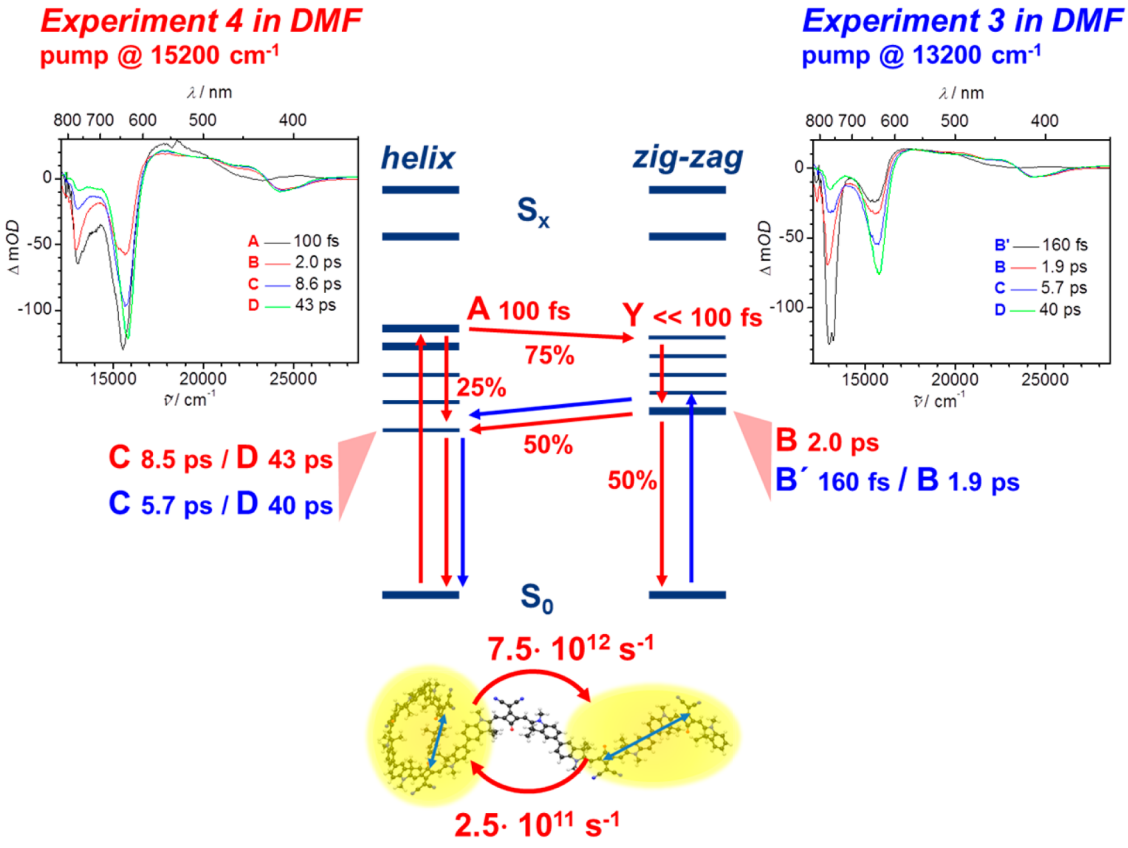

Figure 7. SADS of $[SQB]_n$ in DMF at 15200 (left) and 13200 cm^{-1} (right) pump energy. State diagrams (the number of exciton states is arbitrary) of *helix* and *zigzag* sections (middle). Assignments and data given in red pertain to experiment 4, and those given in blue pertain to experiment 3.

DOI: 10.1021/jacs.5b03644
J. Am. Chem. Soc. 2015, 137, 7851−7861

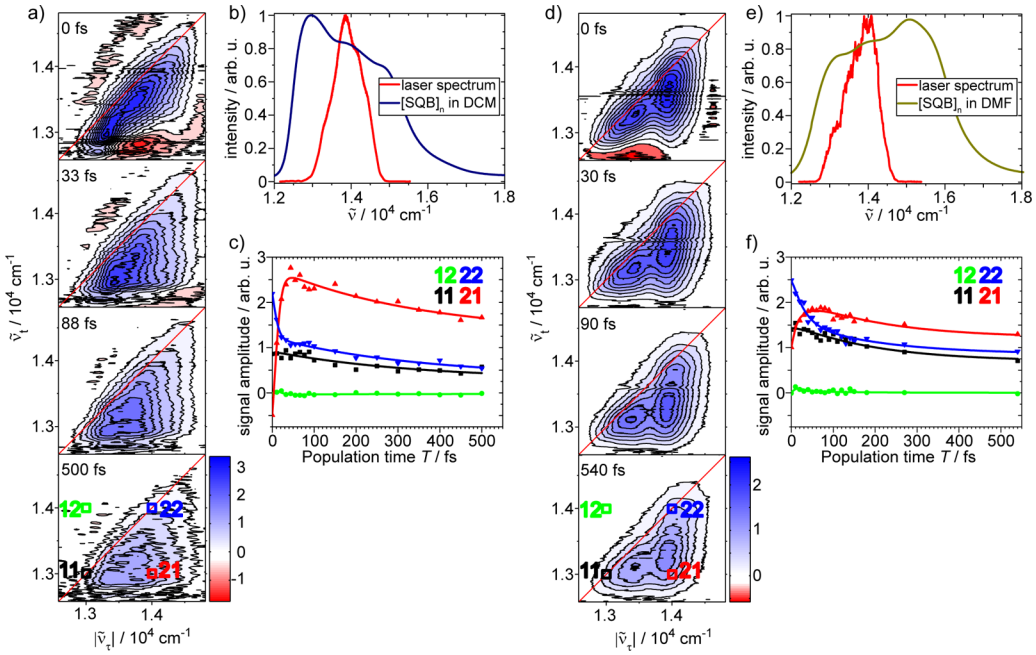

Figure 8. Coherent 2D spectroscopy of $[SQB]_n$ in (a) DCM and (d) DMF for selected population times. 2D spectra have been normalized to the maximum value of the T = 0 fs spectrum and contour lines are drawn in steps of 10% starting from 95%. (b,e) Laser spectrum (red) and absorption spectrum (black) during the 2D scan in DCM (b) and DMF (e). (c,f) Dynamics of the diagonal and off-diagonal signal amplitudes for four regions of interest as marked in the bottom 2D spectrum for $[SQB]_n$ in DCM (c) and DMF (f).

from B′ to D. We assume that this is caused by a broader distribution of *helix* and *zigzag* segments within a polymer strand. Nevertheless, the sequence of SADS indicates energy transfer from excited *zigzag* states to excited *helix* states which we assign to the τ(B) = 1.9 ps step, where the strongest changes in intensity at 13000 and 16000 cm^{-1} are apparent. Again, the spectral differences between the SADS of B′ and of B around 21000−27000 cm^{-1} are associated with changes in ESA upon relaxation within the exciton manifold. This is due to the fact that we excited the sample at the maximum of the lowest energy band which still is somewhat higher in energy than the lowest exciton state.

In experiment 4 where the *helix* segments are primarily excited, we observed a series of SADS with decreasing GSB at ca. 15000 cm^{-1}. At 13000 cm^{-1} the situation is more complicated inasmuch as the GSB displays only a little decrease between the first (black spectrum of A in the left inset in Figure 7) and the second SADS (red spectrum of B in the left inset in Figure 7), but then a rapid decrease until an SADS reflecting purely excited *helix* states has developed (green spectrum of D in the left inset of Figure 7). In analogy to experiment 2, we interpret these findings with an energy transfer from excited *helix* segments to excited *zigzag* segments (τ(A) = 100 fs). From the efficiency of this pathway (75%), we evaluate a rate constant of $k_{A\rightarrow B}$ = 7.5 × 10^{12} s^{-1} for this energy-transfer process, which in turn is followed by ultrafast relaxation within the exciton manifold of the *zigzag* segments to give species B. This excited species has a lifetime of τ = 2.0 ps (very similar to experiment 3 with τ = 1.9 ps) and undergoes back-energy transfer (*zigzag* to *helix* segments) to C with $k_{B\rightarrow C}$ = 2.5 × 10^{12} s^{-1} and an efficiency of 50%. Subsequent relaxation of C into D and depopulation of D into the ground state occurs with τ(C) = 8.5 and τ(D) = 43 ps. At this point we stress that equally good target fits could be obtained by assuming a parallel excitation of *helix* and *zigzag* sections followed by energy transfer from excited *zigzag* to *helix* segments. While we cannot fully rule out this scenario, it appears to be unlikely based on the analysis of experiment 2, where the energy transfer *helix* → *zigzag* is obvious. This energy transfer, for which we obtained an efficiency of 75% in experiment 4, requires that the relaxation within the exciton manifold of the *helix* segments is much slower ($k_{A\rightarrow C}$ = 2.5 × 10^{12} s^{-1}) than the energy-transfer step. Adopting this interpretation also rules out the dotted pathway in experiment 2 (Figure 6) in DCM (see above).

The above outlined analysis results in three major points: First, in DCM the lowest exciton state of *zigzag* segments is lower in energy than the lowest exciton states of *helix* segments. In DMF, the situation is vice versa. Second, relaxation within the exciton manifold of the *helix* segments is much slower than in the *zigzag* segments. And third, energy transfer from the *helix* segments to the *zigzag* structures is an order of magnitude faster than from *zigzag* to *helix* segments.

Concerning point 1: The exciton coupling in a *helix* structure and, consequently the exciton bandwidth, might be larger than in a *zigzag* structure because the individual squaraine chromophores can be closer in the face-to-face arrangement of a helix. The difference of interchromophore distances is sketched in the molecular structure in Figure 6 by blue arrows. Therefore, the electronic structure depends strongly on the supramolecular structure, and a somewhat smaller bandwidth with a higher-lying lowest energy exciton state is expected for, e.g., looser helix arrangements in DCM than in DMF. Both the relaxation within the exciton manifold and the energy-transfer processes (point 2 and 3) depend on a Franck−Condon overlap of states. In general the relaxation within an exciton manifold depends strongly on exciton-vibrational coupling and may also lead to "transient population trapping"[97] in vibrationally excited states. These effects, though hardly predictable in complex systems such as $[SQB]_n$, may influence the relative

DOI: 10.1021/jacs.5b03644
J. Am. Chem. Soc. 2015, 137, 7851−7861

relaxation rates *within* the exciton manifold vs *between* the different polymer sections.

2D Spectroscopy. To visualize the initial interactions and relaxation dynamics between the absorption bands of the polymer, we performed coherent 2D spectroscopy using a laser spectrum covering the absorption maxima at ≈13000 and ≈14000 cm^{-1}. Figure 8 depicts the results for $[SQB]_n$ in DCM (a) and DMF (d) for selected population times T. Excitation corresponds to the horizontal $\tilde{\upsilon}_\tau$ wavenumbers, and detection corresponds to the vertical $\tilde{\upsilon}_t$ wavenumbers. Blue (positive) signals display GSB and SE signal contributions, while red (negative) signals display ESA contributions. This sign convention is opposite to that in transient absorption above because in 2D spectroscopy, one records and plots generally the emitted signal magnitude, rather than the absorbance change. As a consequence of the limited laser pulse bandwidth (Figure 8b for $[SQB]_n$ in DCM and Figure 8e for $[SQB]_n$ in DMF), covering ≈1500 cm^{-1} of the spectrally broad absorption band, the dynamics within these bands are visible as 2D line-shape modifications rather than clearly separated peaks. For the population time T = 0 fs, signal contributions of the solvent have to be taken into account. Furthermore, "phase twist" contributions originating from the temporal overlap of the third pulse with the first two may occur.

The laser pulses centered at 13700 cm^{-1} mainly excite intermediate sections of the polymer which are energetically between the absorption of *zigzag* and *helix* segments. Qualitative similarities can be found in the real-valued 2D spectra of $[SQB]_n$ in DCM and DMF: The T = 0 fs spectrum is mainly elongated along the diagonal for excitation wavenumbers of $|\tilde{\upsilon}_\tau| \lesssim 13750$ cm^{-1}, i.e., excitation and emission frequencies are correlated. For higher excitation wavenumbers, a coupling to lower detection wavenumbers is already observable as a larger shift of the signal below the diagonal. The subsequent dynamics within the first 90 fs are governed by an ultrafast component that is associated with changes in the 2D line shape: At high excitation wavenumbers, the signal loses its amplitude and gains intensity at lower detection wavenumbers. Between 90 and 500 fs, an overall decay of the signal can be observed.

In order to get a better impression of the signal amplitude progression in the 2D spectra, we chose four square regions of interest (ROI) with a side length of ≈115 cm^{-1} centered at the diagonal ($\tilde{\upsilon}_\tau = \tilde{\upsilon}_t$) and off-diagonal ($\tilde{\upsilon}_\tau \neq \tilde{\upsilon}_t$) positions corresponding to absorption maxima at ≈13000 cm^{-1} and ≈14000 cm^{-1}. The signal evolution of these ROIs is shown in Figure 8c for $[SQB]_n$ in DCM and Figure 8f for $[SQB]_n$ in DMF as a function of population time (symbols). Starting at T = 0 fs, the diagonal peaks (11 and 22) have the highest amplitude. With increasing T, the strongest changes are the initial decrease of the 22 peak accompanied by the rise of the corresponding off-diagonal peak 21. After this process, the overall amplitude of all components decreases up to our measurement limit of $T \approx 500$ fs.

To quantify these processes we performed, for each solvent, global fits of the four ROI signals over time, i.e., sharing the rates while amplitudes and offset were free parameters. For $[SQB]_n$ in DCM the fit resulted in two time constants of $1/k$ = 9 ± 2 and 349 ± 118 fs, and in DMF the time constants were $1/k$ = 28 ± 7 and 201 ± 53 fs. In both solvents we observe ultrafast energy transfer from initially excited states toward energetically lower-lying states on the order of our pulse duration. According to the global fit, the cross peak 21 rises with the same time constant as a decay of the corresponding diagonal peak 22. This indicates an ultrafast relaxation within the excitonic manifold toward the lowest states in energy, as was assumed in the global target fit in Figures 6 and 7. From the latter states further relaxation processes occur which lead to an overall decay of the signal without a change in line-shape within our spectral and population time window. The subsequent relaxation displays the relaxation of the *zigzag* segments in DCM with $1/k$ = 349 fs and in DMF with $1/k$ = 201 fs. The time of 349 fs (from the 2D analysis) fits well with the lifetime of B observed in the transient absorption experiment 2, whereas the time of 201 fs in DMF (from the 2D analysis) fits well with the lifetime of B′ in the transient absorption experiment 3.

In the 2D spectroscopy experiments we excited mainly energetically intermediate states of the polymer. In DCM an ultrafast relaxation toward the lowest *zigzag* energy takes place, followed by a further relaxation of this state. In DMF the coupling between intermediate states and *zigzag* states is already visible in the T = 0 fs 2D spectrum as a pronounced off-diagonal signal. Subsequently, the energy relaxes toward the *zigzag* states within $1/k$ = 28 fs, where further relaxation toward the energetically more stable *helix* (in DMF) may occur with $1/k$ = 201 fs. We interpret this as an energy-driven process: In DCM there are mainly *zigzag* segments which are the lowest in energy. The excited intermediate states relax initially toward these *zigzag* states in DCM, while in DMF, the relaxation from the excited intermediate states toward the *helix* segments is coupled via the *zigzag* conformations.

■ CONCLUSIONS

The comparison between experimental and theoretical absorption spectra of squaraine polymers has confirmed that the *zigzag* polymer strands behave like J-aggregates and the *helix* segments like H-aggregates concerning their optically allowed transitions. Based on these structural models, which are to a different degree present in DCM and DMF solutions of $[SQB]_n$, we analyzed the transient absorption measurements and fitted the results to target models which give a consistent picture of all relaxation processes within the exciton manifolds and between the different *helix* and *zigzag* segments within single polymer strands. In addition, the relaxation processes on the subpicosecond time scale were confirmed by 2D spectroscopy. With this information, we could show that excitation of *helix* segments in DCM at higher pump wavenumber is followed by energy transfer to the *zigzag* sections ($k \sim 10^{13}$ s^{-1}). In DMF the situation is somewhat more complex, excitation of the *zigzag* sections at lower pump wavenumber results in energy transfer to *helix* sections, but direct excitation of the *helix* sections at higher wavenumber initiates first an energy transfer to the *zigzag* segments ($k \sim 10^{13}$ s^{-1}), followed by an energy back-transfer to the *helix* sections ($k \sim 10^{11}$ s^{-1}). This shows that energy transfer between different structural sections within one polymer chain is faster than relaxation within the exciton manifold in the present case and supports an assumption made quite recently[33] that energy transfer within polymer chains of squaraines may be well below the subpicosecond time scale. These observations contrast other conjugated polymers such as MEH-PPV, where much slower intrachain energy transfer was found.[3,24] The reason for the very fast energy transfer in squaraine polymers is most likely a matching of the density of states between donor and acceptor states because of a very small reorganization energy in this class

DOI: 10.1021/jacs.5b03644
J. Am. Chem. Soc. 2015, 137, 7851−7861

of cyanine-like chromophores.[33] In the more conventional-type polymers, polyphenylenevinylene and polythiophene, this energy-state matching is obviously weaker as can be seen by a strong Stokes shift and the small spectral overlap of absorption and fluorescence spectra.[98] Thus, if an efficient ultrafast energy transfer is desired, the use of polymers based on cyanine-like chromophores such as squaraines may be advantageous.

■ ASSOCIATED CONTENT

Supporting Information

Transient absorption spectra and global analysis data. The Supporting Information is available free of charge on the ACS Publications website at DOI: 10.1021/jacs.5b03644.

■ AUTHOR INFORMATION

Corresponding Authors

*christoph.lambert@uni-wuerzburg.de
*brixner@phys-chemie.uni-wuerzburg.de

Notes

The authors declare no competing financial interest.

■ ACKNOWLEDGMENTS

We thank the DFG for funding this work within the Research Unit FOR 1809. We also acknowledge support by the European COST Action CM1202 Perspect-H2O and by the SolTech Initiative of the Bavarian State Ministry of Science, Research and the Arts.

■ REFERENCES

(1) Brédas, J.-L.; Beljonne, D.; Coropceanu, V.; Cornil, J. *Chem. Rev.* **2004**, *104*, 4971.
(2) Scholes, G. D. *Annu. Rev. Phys. Chem.* **2003**, *54*, 57.
(3) Hwang, I.; Scholes, G. D. *Chem. Mater.* **2011**, *23*, 610.
(4) Hennebicq, E.; Pourtois, G.; Scholes, G. D.; Herz, L. M.; Russell, D. M.; Silva, C.; Setayesh, S.; Grimsdale, A. C.; Muellen, K.; Bredas, J.-L.; Beljonne, D. *J. Am. Chem. Soc.* **2005**, *127*, 4744.
(5) Beljonne, D.; Pourtois, G.; Silva, C.; Hennebicq, E.; Herz, L. M.; Friend, R. H.; Scholes, G. D.; Setayesh, S.; Mullen, K.; Bredas, J. L. *Proc. Natl. Acad. Sci. U. S. A.* **2002**, *99*, 10982.
(6) Becker, K.; Lupton, J. M. *J. Am. Chem. Soc.* **2006**, *128*, 6468.
(7) Banerji, N. *J. Mater. Chem. C* **2013**, *1*, 3052.
(8) Andrew, T. L.; Swager, T. M. In *Charge and Exciton Transport through Molecular Wires*; Siebbeles, L. D. A., Grozema, F. C., Eds.; Wiley-VCH Verlag GmbH & Co. KGaA: Weinheim, Germany, 2011.
(9) Laquai, F.; Park, Y.-S.; Kim, J.-J.; Basche, T. *Macromol. Rapid Commun.* **2009**, *30*, 1203.
(10) Gadermaier, C.; Lanzani, G. *J. Phys.: Condens. Matter* **2002**, *14*, 9785.
(11) Parkinson, P.; Muller, C.; Stingelin, N.; Johnston, M. B.; Herz, L. M. *J. Phys. Chem. Lett.* **2010**, *1*, 2788.
(12) Grage, M. M. L.; Pullerits, T.; Ruseckas, A.; Theander, M.; Inganas, O.; Sundstrom, V. *Chem. Phys. Lett.* **2001**, *339*, 96.
(13) Grage, M. M. L.; Wood, P. W.; Ruseckas, A.; Pullerits, T.; Mitchell, W.; Burn, P. L.; Samuel, I. D. W.; Sundstrom, V. *J. Chem. Phys.* **2003**, *118*, 7644.
(14) Dykstra, T. E.; Hennebicq, E.; Beljonne, D.; Gierschner, J.; Claudio, G.; Bittner, E. R.; Knoester, J.; Scholes, G. D. *J. Phys. Chem. B* **2009**, *113*, 656.
(15) Schwartz, B. J. *Nat. Mater.* **2008**, *7*, 427.
(16) Becker, K.; Fritzsche, M.; Hoeger, S.; Lupton, J. M. *J. Phys. Chem. B* **2008**, *112*, 4849.
(17) Talipov, M. R.; Boddeda, A.; Timerghazin, Q. K.; Rathore, R. *J. Phys. Chem. C* **2014**, *118*, 21400.
(18) Newbloom, G. M.; Hoffmann, S. M.; West, A. F.; Gile, M. C.; Sista, P.; Cheung, H.-K. C.; Luscombe, C. K.; Pfaendtner, J.; Pozzo, L. D. *Langmuir* **2015**, *31*, 458.
(19) Hoofman, R. J. O. M.; De Haas, M. P.; Siebbeles, L. D. A.; Warman, J. M. *Nature* **1998**, *392*, 54.
(20) Cho, S.; Rolczynski, B. S.; Xu, T.; Yu, L.; Chen, L. X. *J. Phys. Chem. B* **2015**, ASAP. DOI 10.1021/jp5111345.
(21) Ruseckas, A.; Wood, P.; Samuel, I. D. W.; Webster, G. R.; Mitchell, W. J.; Burn, P. L.; Sundstrom, V. *Phys. Rev. B: Condens. Matter Mater. Phys.* **2005**, *72*, 115214/1.
(22) Schwartz, B. J. *Annu. Rev. Phys. Chem.* **2003**, *54*, 141.
(23) Collini, E.; Scholes, G. D. *Science* **2009**, *323*, 369.
(24) Nguyen, T.-Q.; Wu, J.; Doan, V.; Schwartz, B. J.; Tolbert, S. H. *Science* **2000**, *288*, 652.
(25) Consani, C.; Koch, F.; Panzer, F.; Unger, T.; Köhler, A.; Brixner, T. *J. Chem. Phys.* **2015**, *142*, 212429.
(26) Unger, T.; Panzer, F.; Consani, C.; Koch, F.; Brixner, T. *ACS Macro Lett.* **2015**, *4*, 412.
(27) Nguyen, T.-Q.; Doan, V.; Schwartz, B. J. *J. Chem. Phys.* **1999**, *110*, 4068.
(28) Yan, M.; Rothberg, L. J.; Kwock, E. W.; Miller, T. M. *Phys. Rev. Lett.* **1995**, *75*, 1992.
(29) Ruseckas, A.; Theander, M.; Valkunas, L.; Andersson, M. R.; Inganas, O.; Sundstrom, V. *J. Lumin.* **1998**, *76&77*, 474.
(30) Watanabe, A.; Kodaira, T.; Ito, O. *Chem. Phys. Lett.* **1997**, *273*, 227.
(31) Zhang, J. Z.; Kreger, M. A.; Hu, Q. S.; Vitharana, D.; Pu, L.; Brock, P. J.; Scott, J. C. *J. Chem. Phys.* **1997**, *106*, 3710.
(32) Völker, S. F.; Uemura, S.; Limpinsel, M.; Mingebach, M.; Deibel, C.; Dyakonov, V.; Lambert, C. *Macromol. Chem. Phys.* **2010**, *211*, 1098.
(33) Völker, S. F.; Schmiedel, A.; Holzapfel, M.; Renziehausen, K.; Engel, V.; Lambert, C. *J. Phys. Chem. C* **2014**, *118*, 17467.
(34) Völker, S. F.; Dellermann, T.; Ceymann, H.; Holzapfel, M.; Lambert, C. *J. Polym. Sci., Part A: Polym. Chem.* **2014**, *52*, 890.
(35) Völker, S. F.; Schmiedel, A.; Holzapfel, M.; Böhm, C.; Lambert, C. *Phys. Chem. Chem. Phys.* **2013**, *15*, 19831.
(36) Völker, S. F.; Lambert, C. *Chem. Mater.* **2012**, *24*, 2541.
(37) Jiang, J.-Q.; Sun, C.-L.; Shi, Z.-F.; Zhang, H.-L. *RSC Adv.* **2014**, *4*, 32987.
(38) Ajayaghosh, A. *Acc. Chem. Res.* **2005**, *38*, 449.
(39) Beverina, L.; Salice, P. *Eur. J. Org. Chem.* **2010**, 1207.
(40) Sreejith, S.; Carol, P.; Chithra, P.; Ajayaghosh, A. *J. Mater. Chem.* **2008**, *18*, 264.
(41) Yagi, S.; Nakazumi, H. *Top. Heterocycl. Chem.* **2008**, *14*, 133.
(42) Hu, L.; Yan, Z.; Xu, H. *RSC Adv.* **2013**, *3*, 7667.
(43) Beverina, L.; Sassi, M. *Synlett* **2014**, *25*, 477.
(44) Silvestri, F.; Irwin, M. D.; Beverina, L.; Facchetti, A.; Pagani, G. A.; Marks, T. J. *J. Am. Chem. Soc.* **2008**, *130*, 17640.
(45) Merritt, V. Y.; Hovel, H. J. *Appl. Phys. Lett.* **1976**, *29*, 414.
(46) Morel, D. L.; Ghosh, A. K.; Feng, T.; Stogryn, E. L.; Purwin, P. E.; Shaw, R. F.; Fishman, C. *Appl. Phys. Lett.* **1978**, *32*, 495.
(47) Wang, S.; Mayo, E. I.; Perez, M. D.; Griffe, L.; Wei, G.; Djurovich, P. I.; Forrest, S. R.; Thompson, M. E. *Appl. Phys. Lett.* **2009**, *94*, 233304.
(48) Mayerhöffer, U.; Deing, K.; Gruss, K.; Braunschweig, H.; Meerholz, K.; Würthner, F. *Angew. Chem., Int. Ed.* **2009**, *48*, 8776.
(49) Fan, B.; Maniglio, Y.; Simeunovic, M.; Kuster, S.; Geiger, T.; Hany, R.; Nuesch, F. *Int. J. Photoenergy* **2009**, 1.
(50) Wei, G.; Wang, S.; Renshaw, K.; Thompson, M. E.; Forrest, S. R. *ACS Nano* **2010**, *4*, 1927.
(51) Wei, G.; Lunt, R. R.; Sun, K.; Wang, S.; Thompson, M. E.; Forrest, S. R. *Nano Lett.* **2010**, *10*, 3555.
(52) Beverina, L.; Drees, M.; Facchetti, A.; Salamone, M.; Ruffo, R.; Pagani, G. A. *Eur. J. Org. Chem.* **2011**, *2011*, 5555.
(53) Wei, G.-D.; Xiao, X.; Wang, S.-Y.; Zimmerman, J. D.; Sun, K.; Diev, V. V.; Thompson, M. E.; Forrest, S. R. *Nano Lett.* **2011**, *11*, 4261.

DOI: 10.1021/jacs.5b03644
J. Am. Chem. Soc. 2015, 137, 7851−7861

(54) Wang, S.; Hall, L.; Diev, V. V.; Haiges, R.; Wei, G.; Xiao, X.; Djurovich, P. I.; Forrest, S. R.; Thompson, M. E. *Chem. Mater.* **2011**, *23*, 4789.
(55) Wei, G.; Xiao, X.; Wang, S.; Sun, K.; Bergemann, K. J.; Thompson, M. E.; Forrest, S. R. *ACS Nano* **2012**, *6*, 972.
(56) Chen, C.-H.; Cheng, W.-T.; Tsai, M.-L.; Huang, K.-T. *Ind. Eng. Chem. Res.* **2012**, *51*, 3630.
(57) Xiao, X.; Wei, G.; Wang, S.; Zimmerman, J. D.; Renshaw, C. K.; Thompson, M. E.; Forrest, S. R. *Adv. Mater.* **2012**, *24*, 1956.
(58) Deing, K. C.; Mayerhöffer, U.; Würthner, F.; Meerholz, K. *Phys. Chem. Chem. Phys.* **2012**, *14*, 8328.
(59) Kylberg, W.; Zhang, Y.; Aebersold, A.; Araujo de Castro, F.; Geiger, T.; Heier, J.; Kuster, S.; Ma, C.-Q.; Bauerle, P.; Nuesch, F.; Tisserant, J.-N.; Hany, R. *Org. Electron.* **2012**, *13*, 1204.
(60) Maeda, T.; Tsukamoto, T.; Seto, A.; Yagi, S.; Nakazumi, H. *Macromol. Chem. Phys.* **2012**, *213*, 2590.
(61) Bagnis, D.; Beverina, L.; Huang, H.; Silvestri, F.; Yao, Y.; Yan, H.; Pagani, G. A.; Marks, T. J.; Facchetti, A. *J. Am. Chem. Soc.* **2010**, *132*, 4074.
(62) Choi, H.; Kamat, P. V. *J. Phys. Chem. Lett.* **2013**, *4*, 3983.
(63) Maeda, T.; Arikawa, S.; Nakao, H.; Yagi, S.; Nakazumi, H. *New J. Chem.* **2013**, *37*, 701.
(64) Maeda, T.; Hamamura, Y.; Miyanaga, K.; Shima, N.; Yagi, S.; Nakazumi, H. *Org. Lett.* **2011**, *13*, 5994.
(65) Maeda, T.; Nakao, H.; Kito, H.; Ichinose, H.; Yagi, S.; Nakazumi, H. *Dyes Pigm.* **2011**, *90*, 275.
(66) Maeda, T.; Shima, N.; Tsukamoto, T.; Yagi, S.; Nakazumi, H. *Synth. Met.* **2011**, *161*, 2481.
(67) Ros-Lis, J. V.; Martinez-Manez, R.; Sancenon, F.; Soto, J.; Spieles, M.; Rurack, K. *Chem.—Eur. J.* **2008**, *14*, 10101.
(68) Ros-Lis, J. V.; Martinez-Manez, R.; Soto, J. *Chem. Commun.* **2002**, 2248.
(69) Ajayaghosh, A.; Arunkumar, E.; Daub, J. *Angew. Chem., Int. Ed.* **2002**, *41*, 1766.
(70) Radaram, B.; Mako, T.; Levine, M. *Dalton Trans.* **2013**, *42*, 16276.
(71) Ananda Rao, B.; Kim, H.; Son, Y.-A. *Sens. Actuators, B* **2013**, *188*, 847.
(72) Volkova, K. D.; Kovalska, V. B.; Tatarets, A. L.; Patsenker, L. D.; Kryvorotenko, D. V.; Yarmoluk, S. M. *Dyes Pigm.* **2006**, *72*, 285.
(73) Tatarets, A. L.; Fedyunyayeva, I. A.; Dyubko, T. S.; Povrozin, Y. A.; Doroshenko, A. O.; Terpetschnig, E. A.; Patsenker, L. D. *Anal. Chim. Acta* **2006**, *570*, 214.
(74) Terpetschnig, E.; Szmacinski, H.; Ozinskas, A.; Lakowicz, J. R. *Anal. Biochem.* **1994**, *217*, 197.
(75) Thomas, J.; Sherman, D. B.; Amiss, T. J.; Andaluz, S. A.; Pitner, J. B. *Bioconjugate Chem.* **2007**, *18*, 1841.
(76) Renard, B.-L.; Aubert, Y.; Asseline, U. *Tetrahedron Lett.* **2009**, *50*, 1897.
(77) Gao, F.-P.; Lin, Y.-X.; Li, L.-L.; Liu, Y.; Mayerhöffer, U.; Spenst, P.; Su, J.-G.; Li, J.-Y.; Würthner, F.; Wang, H. *Biomaterials* **2014**, *35*, 1004.
(78) Arunkumar, E.; Fu, N.; Smith, B. D. *Chem.—Eur. J.* **2006**, *12*, 4684.
(79) Gassensmith, J. J.; Arunkumar, E.; Barr, L.; Baumes, J. M.; DiVittorio, K. M.; Johnson, J. R.; Noll, B. C.; Smith, B. D. *J. Am. Chem. Soc.* **2007**, *129*, 15054.
(80) Xiang, Z.; Nesterov, E. E.; Skoch, J.; Lin, T.; Hyman, B. T.; Swager, T. M.; Bacskai, B. J.; Reeves, S. A. *J. Histochem. Cytochem.* **2005**, *53*, 1511.
(81) Müllen, K.; Wegner, G. *Electronic Materials: The Oligomer Approach*; Wiley-VCH: Weinheim, Germany, 1998.
(82) Lambert, C.; Scherpf, T.; Ceymann, H.; Schmiedel, A.; Holzapfel, M. *J. Am. Chem. Soc.* **2015**, *137*, 3547.
(83) Cabanillas-Gonzalez, J.; Grancini, G.; Lanzani, G. *Adv. Mater.* **2011**, *23*, 5468.
(84) Mukamel, S. In *Oxford Series in Optical and Imaging Sciences*; Lapp, M., Nishizawa, J.-I., Snavely, B. J., Stark, H., Tam, A. C., Wilson, T., Eds.; Oxford University Press: New York, 1995; Vol. *6*, p 209.
(85) Mukamel, S. *Annu. Rev. Phys. Chem.* **2000**, *51*, 691.
(86) Jonas, D. M. *Annu. Rev. Phys. Chem.* **2003**, *54*, 425.
(87) Cho, M. *Chem. Rev.* **2008**, *108*, 1331.
(88) Van Stokkum, I. H. M.; Larsen, D. S.; Van Grondelle, R. *Biochim. Biophys. Acta, Bioenerg.* **2004**, *1657*, 82.
(89) Snellenburg, J. J.; Laptenok, S. P.; Seger, R.; Mullen, K. M.; Stokkum, I. H. M. v. *J. Stat. Soft.* **2012**, *49*, 1.
(90) Mullen, K. M.; Stokkum, I. H. M. v. *J. Stat. Soft.* **2007**, *18*, 1.
(91) Snellenburg, J. J.; Dekker, J. P.; van Grondelle, R.; van Stokkum, I. H. M. *J. Phys. Chem. B* **2013**, *117*, 11363.
(92) Selig, U.; Langhojer, F.; Dimler, F.; Lohrig, T.; Schwarz, C.; Gieseking, B.; Brixner, T. *Opt. Lett.* **2008**, *33*, 2851.
(93) Humeniuk, A.; Mitric, R. 2015, arXiv:1503.01714.
(94) Yanai, T.; Tew, D. P.; Handy, N. C. *Chem. Phys. Lett.* **2004**, *393*, 51.
(95) Niehaus, T. A.; Suhai, S.; Della Sala, F.; Lugli, P.; Elstner, M.; Seifert, G.; Frauenheim, T. *Phys. Rev. B: Condens. Matter Mater. Phys.* **2001**, *63*, 085108/1.
(96) Elstner, M.; Porezag, D.; Jungnickel, G.; Elsner, J.; Haugk, M.; Frauenheim, T.; Suhai, S.; Seifert, G. *Phys. Rev. B: Condens. Matter Mater. Phys.* **1998**, *58*, 7260.
(97) Polyutov, S.; Kuehn, O.; Pullerits, T. *Chem. Phys.* **2012**, *394*, 21.
(98) Gaab, K. M.; Bardeen, C. J. *J. Phys. Chem. B* **2004**, *108*, 4619.

DOI: 10.1021/jacs.5b03644
J. Am. Chem. Soc. 2015, 137, 7851−7861